Subband Structure of Silicon Nanowires from the Hensel-Hasegawa-Nakayama Model

Z. Stanojević, O. Baumgartner, V. Sverdlov and H. Kosina

***Abstract*—The subband structure of nanowires is commonly obtained through an atomistic tight binding approach. In this work an alternative, continuum based method is investigated, namely a two-band $\mathbf{k}\cdot\mathbf{p}$ approximation of the conduction band structure. A derivation of the subband Schrödinger equations from the bulk model and their numerical solution are presented for [100] nanowires. Self-consistent simulation results of exemplary devices are examined and the influence of confinement on the band structure is discussed. For nanowire thicknesses below ten nanometers band structure effects similar to those observed using atomistic models become apparent.**

***Index Terms*—Two-band $\mathbf{k}\cdot\mathbf{p}$ model, quantum confinement, subband structure, self-consistent solution, silicon nanowires**

I. Introduction

Short channel effects are viewed as one of the main obstacles to further scaling of device dimensions. In order to remedy these effects, multigate, gate-all-around, and nanowire (NWFET) structures are currently under investigation. Such structures promise improved electrostatic control of the channel. However, due to the small cross sections, quantization effects have to be carefully considered.

In this paper, a continuum approach based on the $\mathbf{k}\cdot\mathbf{p}$ theory is presented. The bulk Hamiltonian is extended to take two dimensional confinement into account. Also, the principles of discretizing the Hamiltonian for numerical simulation are explained. Band structure and wavefunctions are obtained by diagonalizing the Hamiltonian for different electron wavenumbers $k_\|$ along the nanowire axis. From these results, the density of states, electron concentration and effective mass are extracted.

The paper is structured as follows: In Section II the model Hamiltonian is described as well as its adaptation to the nanowire problem. Section III gives an overview of the discretization scheme and discusses numerical integration of the electron distribution over $k_\|$-space. In Section IV the simulation setup and the particular devices under investigation are described, while in Section V the results are discussed and compared to the results obtained from other models.

II. Model

In order to capture the band structure effects occurring in nanowires one must start with an accurate description of the bulk band structure. For silicon, the Hensel-Hasegawa-Nakayama model [1] provides such a description and will thus be used in this work. The model utilizes a two-band $\mathbf{k}\cdot\mathbf{p}$ Hamiltonian, which represents a first-order expansion of the lowest conduction band valleys around the X-points.

$$\mathbf{H} = \left(\frac{\hbar^2(k_{t1}^2+k_{t2}^2)}{2m_\mathrm{t}} + \frac{\hbar^2 k_l^2}{2m_\mathrm{l}}\right)\mathbf{I} + \frac{\hbar^2 k_0 k_l}{m_\mathrm{l}}\sigma_x - \frac{\hbar^2 k_{t1}k_{t2}}{M}\sigma_z + V\mathbf{I} \tag{1}$$

Here V denotes the potential, i.e. the conduction band edge; $m_\mathrm{l} = 0.916 m_e$ and $m_\mathrm{t} = 0.196 m_e$ are the longitudinal and transversal effective masses and $\frac{1}{M} \approx \frac{1}{m_\mathrm{t}} - \frac{1}{m_e}$; $k_0 = 0.15\frac{2\pi}{a}$ amounts to the distance between the X-point and the corresponding valley minima; $\sigma_{x,z}$ denote the Pauli matrices and $\mathbf{I}$ the 2×2 identity matrix.

The electrons are confined to the cross section of the nanowire, which is assumed parallel to the x, y plane, while they can move quasi-freely in the z direction or along the nanowire axis. In order to modify the model to describe confined electrons, two out of three k-components are replaced by derivatives [2]. Since three valley pairs exist in silicon (two unprimed, one primed), three different mappings apply,

$$\vec{k}^{\mathbf{1}} = \begin{bmatrix} k_\| \\ -i\partial_x \\ -i\partial_y \end{bmatrix}, \vec{k}^{\mathbf{2}} = \begin{bmatrix} -i\partial_y \\ k_\| \\ -i\partial_x \end{bmatrix}, \vec{k}' = \begin{bmatrix} -i\partial_x \\ -i\partial_y \\ k_\| \end{bmatrix}, \tag{2}$$

resulting in three different sets of terms for H_{11}, H_{12}, H_{21} and H_{22}:

$$\begin{aligned} H^{\mathbf{1}}_{11,22} &= \frac{\hbar^2 k_\|^2}{2m_\mathrm{t}} - \frac{\hbar^2\partial_y^2}{2m_\mathrm{t}} - \frac{\hbar^2\partial_x^2}{2m_\mathrm{l}} \pm i\frac{\hbar^2 k_0\partial_x}{m_\mathrm{l}} + V \\ H^{\mathbf{1}}_{12,21} &= -i\frac{\hbar^2 k_\|\partial_y}{M} \end{aligned} \tag{3}$$

$$\begin{aligned} H^{\mathbf{2}}_{11,22} &= \frac{\hbar^2 k_\|^2}{2m_\mathrm{t}} - \frac{\hbar^2\partial_x^2}{2m_\mathrm{t}} - \frac{\hbar^2\partial_y^2}{2m_\mathrm{l}} \pm i\frac{\hbar^2 k_0\partial_y}{m_\mathrm{l}} + V \\ H^{\mathbf{2}}_{12,21} &= -i\frac{\hbar^2 k_\|\partial_x}{M} \end{aligned} \tag{4}$$

$$H'_{11,22} = -\frac{\hbar^2(\partial_x^2+\partial_y^2)}{2m_\mathrm{t}} + \frac{\hbar^2 k_\parallel^2}{2m_\mathrm{l}} \mp \frac{\hbar^2 k_0 k_\parallel}{m_\mathrm{l}} + V$$
$$H'_{12,21} = \frac{\hbar^2 \partial_x \partial_y}{M}. \quad (5)$$

III. Numerical Approach

The partial derivatives in (3) through (5) are discretized using box integration and applying Gauss' law, resulting in the following transformations:

$$\int_{\mathscr{A}} \mathrm{d}A \left(\frac{\hbar^2\partial_x^2}{2m_\mathrm{t}} + \frac{\hbar^2\partial_y^2}{2m_\mathrm{l}}\right) = \oint_{\partial\mathscr{A}} \mathrm{d}s \frac{\hbar^2}{2}\vec{n}\cdot\begin{bmatrix}1/m_\mathrm{t} & 0\\ 0 & 1/m_\mathrm{l}\end{bmatrix}\cdot\vec{\nabla} \quad (6)$$

$$\int_{\mathscr{A}} \mathrm{d}A \frac{\hbar^2 k_0 \partial_x}{2m_\mathrm{l}} = \oint_{\partial\mathscr{A}} \mathrm{d}l \frac{\hbar^2 k_0 \vec{n}\cdot\vec{e}_x}{m_\mathrm{l}} \quad (7)$$

$$\int_{\mathscr{A}} \mathrm{d}A \frac{\hbar^2 k_\parallel \partial_x}{2m_\mathrm{l}} = \oint_{\partial\mathscr{A}} \mathrm{d}l \frac{\hbar^2 k_\parallel \vec{n}\cdot\vec{e}_x}{m_\mathrm{l}} \quad (8)$$

$$\int_{\mathscr{A}} \mathrm{d}A \frac{\hbar^2(\partial_x^2+\partial_y^2)}{2m_\mathrm{t}} = \oint_{\partial\mathscr{A}} \mathrm{d}l \frac{\hbar^2 \vec{n}\cdot\vec{\nabla}}{2m_\mathrm{t}} \quad (9)$$

$$\int_{\mathscr{A}} \mathrm{d}A \frac{\hbar^2 \partial_x \partial_y}{2M} = \oint_{\partial\mathscr{A}} \mathrm{d}l \frac{\hbar^2}{M}\vec{n}\cdot\begin{bmatrix}0 & 1\\ 1 & 0\end{bmatrix}\cdot\vec{\nabla}. \quad (10)$$

The boxes are laid out on a non-uniform rectangular grid. The gradients at the box interfaces are evaluated by taking into account the central points of all six boxes adjacent to the respective interface, while the scalar quantities at the interfaces are evaluated by averaging their values at the central points of the boxes at either side of the interface (Figure 1).

Taking the above considerations into account, the eigenvalue problem

$$\mathbf{H}^{\mathbf{1,2,}\prime}(k_\parallel)\begin{bmatrix}\psi_1\\ \psi_2\end{bmatrix} = E\begin{bmatrix}\psi_1\\ \psi_2\end{bmatrix} \quad (11)$$

is discretized and solved using standard LAPACK routines. This is done for a set of $k_\parallel$-values, given by a $k_\parallel$-grid. The electron concentration is then computed by numerical quadrature of the wavefunctions along the $k_\parallel$-grid according to

$$n = \sum_s \int_{-\infty}^{\infty} \frac{\left|\psi_{1,s}(k_\parallel)\right|^2 + \left|\psi_{2,s}(k_\parallel)\right|^2}{1+\exp\left(\frac{E_s(k_\parallel)-E_\mathrm{F}}{k_\mathrm{B}T}\right)}\frac{\mathrm{d}k_\parallel}{\pi}, \quad (12)$$

where s denotes the subband index. Finally, the two-band $\mathbf{k}\cdot\mathbf{p}$ model is evaluated self-consistently with the Poisson equation.

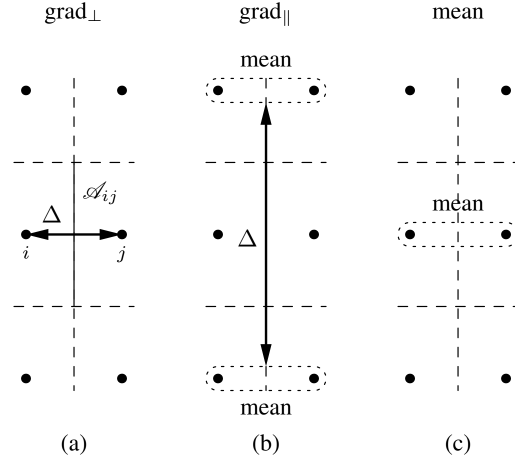

Fig. 1. Evaluation scheme for (a) the component of the gradient perpendicular to a box boundary, (b) the in-plane component of the gradient and (c) the value of a quantity at the surface itself

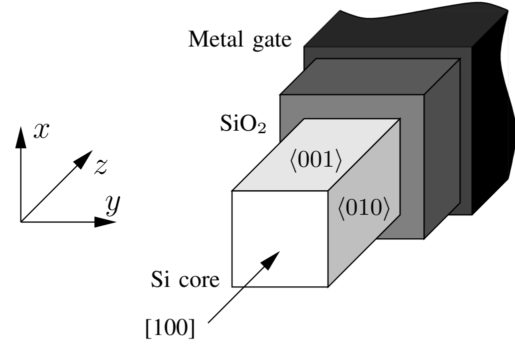

Fig. 2. Device structure of the silicon NWMOS

IV. Exemplary Devices

The devices under study are nanowires made of intrinsic silicon grown in [100] direction. Their cross section is of square shape with a cross section area ranging from 4nm^2 to 49nm^2. The nanowires are surrounded by an all-around gate structure with a 1nm thick SiO_2-layer and a metal gate, through which a bias voltage of 1V is applied. The device structure is displayed in Figure 2.

V. Results and Discussion

A. Subband Structure

Figure 3 and 4 show the subband structure of the 5nm and 2nm devices, respectively. The confinement projects the unprimed valleys onto the Γ-point ($k_\parallel = 0$) and causes a warping of the subbands, an effect which could not be captured by simple effective mass calculations. Most notably, the inverse curvature, i.e. the effective mass, of the unprimed subbands increases significantly for small thicknesses. Figure 5 shows the effective mass change over nanowire cross section

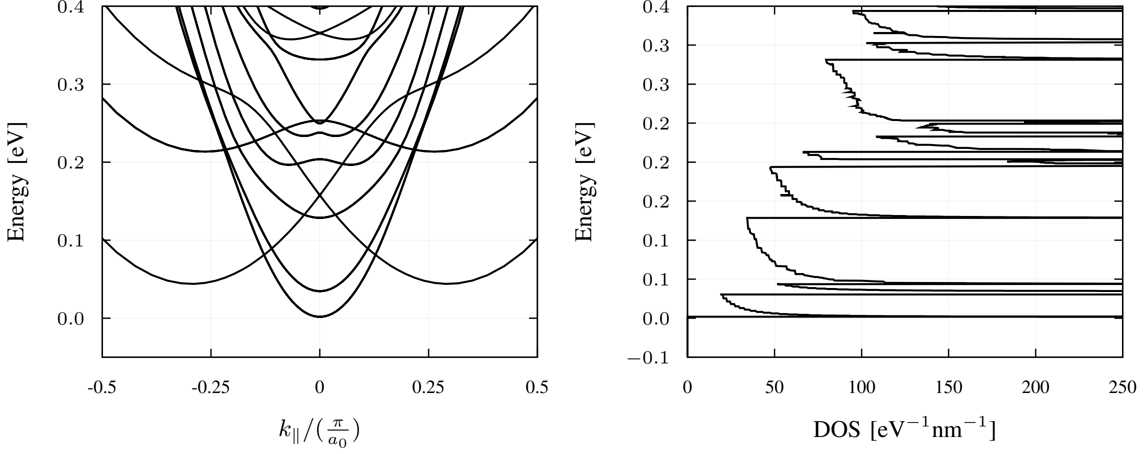

Fig. 3. Subband structure and density of states for the 5nm device

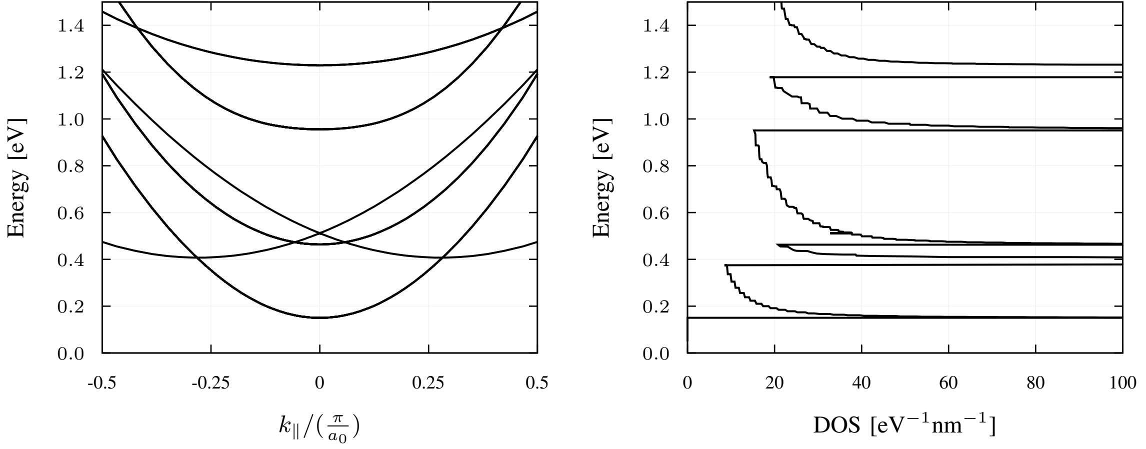

Fig. 4. Subband structure and density of states for the 2nm device

area. For comparison, data from Wang et. al. [3] and Zheng et. al. [4] obtained through the atomistic tight binding approach is plotted as well. As can be clearly seen, the effective mass calculated by two-band $\mathbf{k}\cdot\mathbf{p}$ follows the same law as found by the other authors. However, the two-band $\mathbf{k}\cdot\mathbf{p}$ model slightly overestimates the effective mass increase with respect to the tight binding data. Although it appears that the effective mass curve obtained here is shifted towards higher effective mass as a whole, it still asymptotically approaches the bulk value of 0.196 for large cross section areas. The effective mass curve can be fitted using a power law,

$$\frac{m_{\|}^{*}}{m_{\mathrm{t,bulk}}} = \left(\frac{A}{A_0}\right)^{\alpha}, \tag{13}$$

with an estimated exponent $\alpha = -0.72$. The dependence of the effective mass with respect to the gate bias was investigated as well, however it was found to be negligible; it changes by less than one percent for $V_{\mathrm{gate}} = 0 \ldots 1V$.

The offset of the conduction band due to confinement is plotted in Figure 6. The energy distance between unprimed and primed bands increases for small widths due to different quantization masses, which means that for very thin nanowires only the lower unprimed subbands are effectively populated.

B. Electron Concentration

The electron concentration of the 5nm and 2nm device are plotted in Figure 7 and 8, respectively. In both figures the electron concentration obtained from the two-band $\mathbf{k}\cdot\mathbf{p}$ model is compared to the one produced by effective mass calculations. While the difference between the models is negligible in the 5nm case, for the 2nm device the two-band $\mathbf{k}\cdot\mathbf{p}$ model predicts a higher concentration which is due to

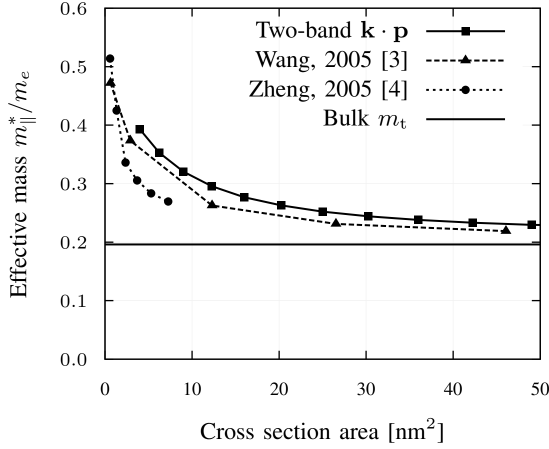

Fig. 5. Effective mass of the lowest subband (unprimed) plotted against cross section area

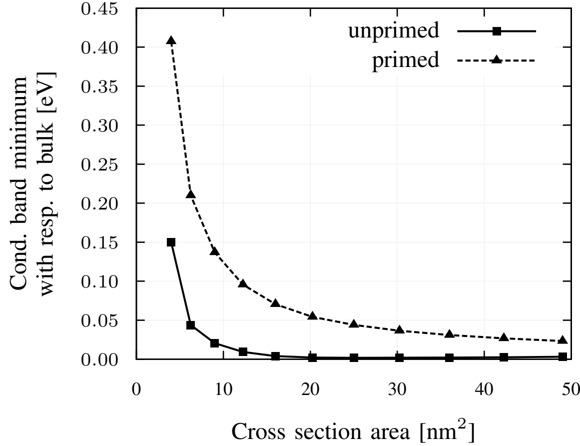

Fig. 6. Conduction band valley minimum dependence on cross section area

the effective mass increase discussed in the previous section.

VI. Summary and Conclusion

The Hensel-Hasegawa-Nakayama model was adapted for calculation of silicon nanowire band structures. It was demonstrated that by introducing only one additional model parameter, M, a far more accurate band structure can be obtained compared to the simple effective mass approach. The simulated band structure displays important features such as subband warping and effective mass increase for small thicknesses. The latter effect was found to agree reasonably well with results obtained from atomistic tight binding simulations.

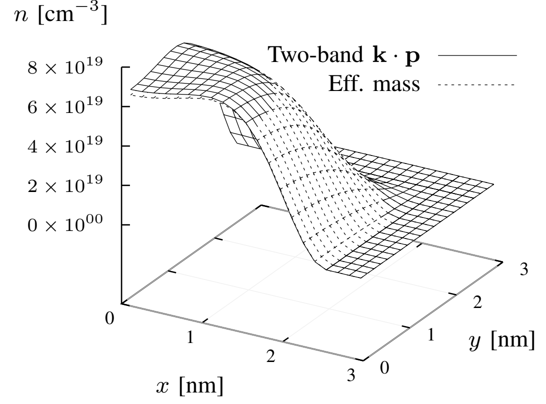

Fig. 7. Electron concentration of the 5nm device

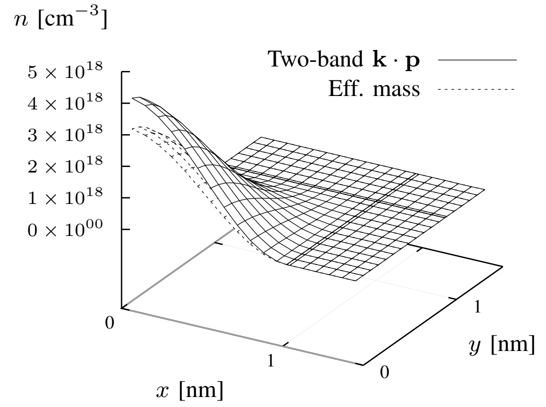

Fig. 8. Electron concentration of the 2nm device

Acknowledgment

This work has been supported by the Austrian Science Fund, special research program IR-ON (F2509).

References

[1] J. C. Hensel, H. Hasegawa, and M. Nakayama, "Cyclotron resonance in uniaxially stressed silicon. II. nature of the covalent bond," *Phys. Rev.*, vol. 138, no. 1A, pp. A225–A238, Apr 1965.

[2] O. Baumgartner, M. Karner, V. Sverdlov, and H. Kosina, "Electron subband structure in strained silicon UTB films from the Hensel-Hasegawa-Nakayama model - part 2 efficient self-consistent numerical solution of the k · p Schrödinger equation," *Solid-State Electronics*, vol. In Press, Corrected Proof. [Online]. Available: http://www.sciencedirect.com/science/article/B6TY5-4Y1WK4B-3/2/785a47c4eb1ec975b69102c8468a5d51

[3] J. Wang, A. Rahman, A. Ghosh, G. Klimeck, and M. Lundstrom, "On the validity of the parabolic effective-mass approximation for the I-V calculation of silicon nanowire transistors," *Electron Devices, IEEE Transactions on*, vol. 52, no. 7, pp. 1589–1595, July 2005.

[4] Y. Zheng, C. Rivas, R. Lake, K. Alam, T. Boykin, and G. Klimeck, "Electronic properties of silicon nanowires," *Electron Devices, IEEE Transactions on*, vol. 52, no. 6, pp. 1097–1103, June 2005.